Cellular and Molecular Biology
E-ISSN : 1165-158X / P-ISSN : 0145-5680
www.cellmolbiol.org

Identification of anoikis-related subtypes and construction of the prognostic model in hepatocellular carcinoma

Wanzhi Fang[1], Zhong Chen[2*]

[1] Nantong university, Nantong 226001, China
[2] Department of Hepatobiliary Surgery, Affiliated Hospital of Nantong University, Nantong 226001, China

ARTICLE INFO

Original paper

Article history:
Received: July 28, 2023
Accepted: August 02, 2023
Published: September 30, 2023

Keywords:

Hepatocellular carcinoma, anoikis, prognosis, bioinformatics analysis

ABSTRACT

Anoikis resistance, which enables tumor cells to survive detachment-induced cell death, plays a crucial role in cancer growth and metastasis. In hepatocellular carcinoma (HCC), understanding the molecular basis of anoikis resistance is essential for developing effective treatments. This study aims to identify HCC subtypes based on anoikis gene expression, construct a prognostic signature, and explore treatment responses according to patient risk. Using the TCGA tumor database, we analyzed differential gene expression between HCC and adjacent tissues. Through consensus clustering on anoikis apoptotic genes, two distinct molecular subtypes were identified, showing significant prognostic differences. We further performed principal component analysis and survival difference analysis on these subtypes. Additionally, we analyzed immune cellular infiltration using various tools. From univariate Cox screening, we identified 13 key prognostic genes among differentially expressed genes between subtypes. Using the LASSO Cox algorithm, we constructed a prognostic model based on these characteristic genes. The model's performance was evaluated using training and verification sets, categorizing patients into high and low-risk groups based on the model's median score. Survival differences were compared between these groups. Univariate and multivariate Cox analyses confirmed the independence of the signature genes as prognostic factors. Finally, we predicted relevant molecular responses and potential drug treatment effects. Dysregulation of most anoikis genes was observed in the TCGA-LIHC cohort, and the identified molecular subtypes displayed distinct prognostic outcomes. The constructed prognostic model demonstrated superior predictive performance, with better drug efficacy prediction in the low-risk group. In conclusion, this study developed a robust prognostic model for HCC based on anoikis-related genes, providing valuable insights for personalized treatment strategies. The identified key prognostic genes and their mechanisms offer potential targets for targeted therapies against anoikis resistance in HCC.

Doi: http://dx.doi.org/10.14715/cmb/2023.69.9.34 Copyright: © 2023 by the C.M.B. Association. All rights reserved.

Introduction

Liver cancer is a prevalent cancer that accounts for about 50% of annual liver cancer deaths worldwide, with hepatocellular carcinoma(HCC) accounting for about 90% (1). Although surgery remains a primary treatment option, liver cancer is often diagnosed at an advanced stage, with a high degree of malignancy (2). Even with radical surgical resection, the recurrence rate after surgery is high, and the five-year survival rate is less than 30% (3). Therefore, it is crucial to conduct in-depth research on the mechanism of liver cancer occurrence and development to identify new screening indicators, therapeutic targets, and prognostic indicators.

Anoikis is a programmed cell apoptosis triggered by the detachment of cells from the extracellular matrix (4). It plays a crucial role in body development, tissue homeostasis, disease occurrence, and tumor metastasis (5). Under normal conditions, anoikis prevents the growth and spread of abnormal cells. However, cancer cells can resist anoikis, leading to aggressive metastasis and the spread of cancer (4, 6). Anoikis resistance is a natural molecular prerequisite for the aggressive metastatic spread of cancer. Therefore, understanding the interaction between cells and extracellular matrix and the regulation mechanism of anoikis is crucial for in-depth understanding of the occurrence and development of cancer and for cancer treatment research.

In this study, we analyzed 34 genes related to anoikis using the TCGA tumor database and calculated the differential expression between liver cancer and paracancerous tissues using limma. We constructed a PPI network for gene GO enrichment analysis using the STRING database. Using consensus clustering analysis based on anoikis genes and TCGA tumor sample data as a training set, we identified molecular subtypes and divided the TCGA liver cancer samples into two subtypes. There were significant prognostic differences between the subtypes. We analyzed the infiltration of immune cells using CIBERSORT, XCELL, SSGSEA, and TIMER based on the training set data. We performed univariate Cox screening of prognosis-related genes using differentially expressed genes between subtypes. We constructed a characteristic gene by removing redundant genes using LASSO Cox based on the prognosis genes and obtained 13 key prognostic genes. We analyzed the prognostic efficacy through the training set

* Corresponding author. Email: chenz9806@163.com

and verification and divided the group into high and low-risk groups, comparing the survival difference. We verified that the characteristic gene was an independent prognostic factor using univariate and multivariate Cox. Finally, we predicted the relevant molecular responses and the effect of drug treatment and found that drug treatment had better predictive performance in the high-risk group.

Materials and Methods

Dataset preparation and preprocessing analysis data.

This study utilized tumor and paracancerous tissues from 363 patients in the TCGA database, with 165 cases under the age of 60 and 198 cases over the age of 60, 118 cases of women, and 245 cases of men. Additionally, data from 44 cases, including 20 cases over 60 years old, 6 cases of women, and 58 cases of men were included. Transcriptome data of 28 immune cell types were collected from a related study. The Gene Expression Omnibus (GEO) and The Cancer Genome Atlas (TCGA) public gene expression data were searched for complete clinical annotations for hepatocellular carcinoma (LIHC). RNA-sequencing data of gene expression (FPKM values) and clinical information were downloaded for the TCGA dataset using the R package 'TCGAbiolinks', and the data of HCC were selected according to the clinical information. The gene expression matrix file for GSE116174 was downloaded from the GEO database (http://www.ncbi.nlm.nih.gov/geo/). The Illumina sequencing probe annotation files are available under GPL13158. The TCGA_LIHC and GSE116174 data undergo the following steps of processing: (1) Probes are converted to gene signatures; (2) Probes corresponding to multiple genes are removed; (3) For expressions with multiple gene signatures, the median value of the case is taken. The preprocessed TCGA-LIHC data includes 363 cases of cancer tissue and 50 cases of paracancerous tissue samples. Anoikis-related genes were obtained from the MSigDBv7.5.1 database, totaling 34 genes.

Differential Expression Analysis

Differential expression analysis was performed on HCC tumor tissues and paracancerous tissues using the 'limma' package in R. The differentially expressed genes were filtered based on FDR <0.01, and volcano and heat maps were generated using the R packages 'ggplot2' and 'ComplexHeatmap'. Boxplots between clinical characteristics were drawn using ggplot2, and the P value of the difference between the two groups was calculated using the Wilcoxon rank sum test. The Kruskal-Wallis test was used to calculate the P value between multiple groups. A statistically significant difference was defined as P<0.05.

Protein-protein interaction (PPI) network analysis

To perform PPI network analysis, we utilized the STRING database (https://string-db.org/), which is a comprehensive online database of known and predicted protein interactions. The interactions included both physical and functional associations and were derived from a variety of sources, including computational predictions, high-throughput experiments, automated text mining, and co-expression networks. We then mapped the anoikis death-related genes onto the PPI network, setting an interaction score threshold of >0.4.

Consistent clustering

To explore the role of apoptosis-related genes in HCC, we employed the 'ConsensusClusterPlus' software package, utilizing 1000 iterations and an 80% resampling rate, with the Pam method and Spearman distance to classify HCC patients into four distinct subtypes. We then utilized the Kaplan-Meier method to generate survival curves and compared survival differences between the different subgroups.

Construction and validation of the prognostic signature for HCC patients

In this study, the limma package in R was used to calculate the differentially expressed genes (DEG) |log2FC| > 0.585 and FDR < 0.01 of different molecular subtypes as the screening criteria for differential expression. Subsequently, genes associated with prognosis were screened using univariate Cox analysis for subtype differentially expressed genes. LASSO regression analysis was then used to reduce multicollinearity and identify important genes for constructing prognostic models. The normalized expression matrix of genes was used as the independent variable in the regression, while the dependent variables were overall survival and patient status in the TCGA cohort. The risk score of the patient was calculated based on the expression level of the gene and its corresponding regression coefficient:

$$Risk\ score = \sum_{i=1}^{n} (exp_i * \beta_i)$$

The study analyzed the prognostic value of n genes, with expi representing the expression value of gene i and βi representing its regression coefficient. Patients were categorized into high-risk and low-risk groups based on the median risk score, and the 'survminer' package was utilized to compare the survival difference in OS between the two groups. The 'timeROC' package was used to assess the predictive value of prognostic features through time-dependent ROC curve analysis. Univariate and multivariate Cox analyses were conducted to examine the independent prognostic value of the risk score. The same formula was employed to calculate the risk score in the validation cohort.

Enrichment analysis

GO analysis is a widely used bioinformatics tool for annotating genes and their products, which includes three categories: cellular components (CC), molecular functions (MF), and biological pathways (BP). KEGG is a collection of databases that provide information on genomes, biological pathways, diseases, and chemicals. In this study, we utilized the clusterProfiler package to perform GO functional enrichment analysis and KEGG pathway analysis on differentially expressed genes between anoikis subtypes of hepatocellular carcinoma, in order to predict their potential molecular functions. P < 0.05 was considered to demonstrate statistically significant differences.

Estimation of immune cell infiltration in the tumor microenvironment

In this study, we utilized the ssGSEA algorithm to quantify the relative abundance of cellular infiltrates in the HCC tumor microenvironment (TIME). To identify infiltrating immune cell types, we used a gene set obtained

from Charoentong's research (PMID: 28052254), which is enriched in various human immune cell subtypes, such as activated CD8+ T cells, activated dendritic cells, macrophages, natural killer T cells, and regulatory T cells. To calculate the stromal score, immune score, and tumor purity score, we utilized the 'ESTIMATE' package in R.

Predicting drug sensitivity

We utilized the GDSC Cancer Genomics Drug Sensitivity Database to determine the drug IC50 value of each sample in the training set using the calcPhenotype algorithm of the R package oncoPredict. Spearman correlation was calculated to evaluate the correlation between small molecule drug sensitivity and risk score. Additionally, we compared the difference in small molecule drug IC50 between high and low risk score groups.

Statistical analysis

The statistical analysis was conducted using R language (version 4.1.2). Survival curves were created using the Kaplan-Meier method, and group differences were compared using the log-rank test. Univariate and multivariate Cox regression models were utilized in combination with clinical features to determine the independent prognostic value of the risk score. The ROC curves were used to estimate the predictive efficiency of risk models for 1-, 3-, and 5-year OS. A P value of less than 0.05 was considered statistically significant.

Results

Dysregulation of anoikis gene expression in hepatocellular carcinoma

The study analyzed 363 patient tumor tissue samples and 50 paracancerous tissue samples from TCGA-LIHC. The differential expression of anoikis-related genes in paracancerous tissues and tumor tissues was counted, revealing extensive-expression disorders in the TCGA-LIHC cohort. Most of the anoikis genes showed a significant effect on tumor progression, either promoting or inhibiting it. These findings demonstrate the practical significance of researching the role of anoikis genes in hepatocellular carcinoma, as is shown in Figure 1.

In the TCGA-LIHC cohort, we investigated the expression of anoikis-related genes in different clinical groups of LIHC patients. Our findings revealed that the expression of these genes varied across different age groups, sex groups, and clinical stages (clinical stage I/II and clinical stage III/IV), as is shown in Figure 2. To further explore the interaction of these genes, we constructed a PPI network based on anoikis-related genes using the STRING database. Our results indicated that SRC, STK11, and PIK3CA were highly correlated in the network, suggesting that these genes may play a crucial role in the anoikis resistance of HCC tumor cells, as shown in Figure 3A. Additionally, GO enrichment analysis revealed that anoikis-related genes were primarily involved in tumor resistance to anoikis and tumor drug

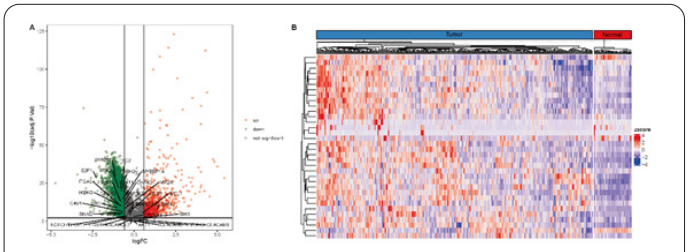

Figure 1. (A) displays the changes in expression levels of anoikis genes in TCGA-LIHC samples, comparing low expression to high expression. (B) is a heat map that illustrates the difference in expression levels of anoikis genes between TCGA-LIHC cancerous tissues and non-cancerous tissues.

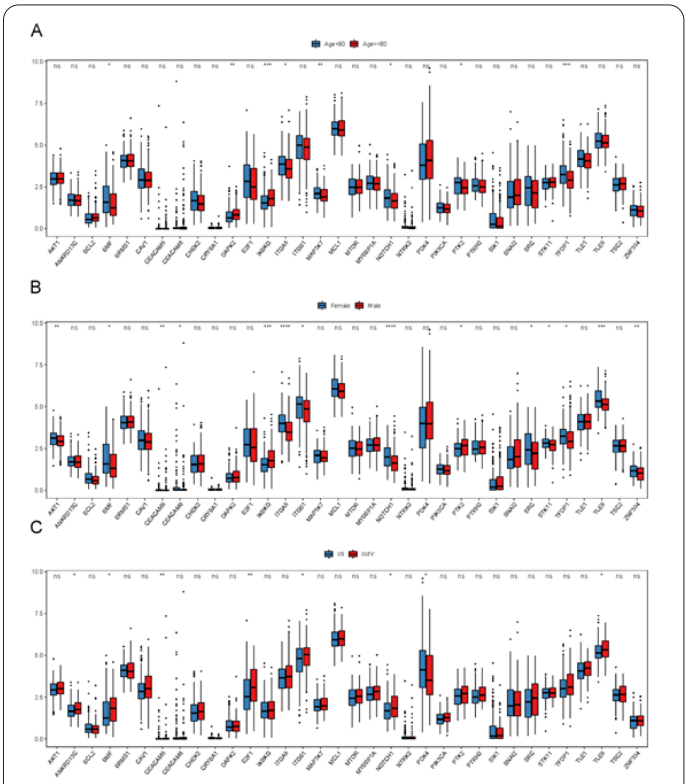

Figure 2. The figure displays the differential expression of genes related to anoikis in different clinical feature groups, including (A) age, (B) sex, and (C) clinical stage.

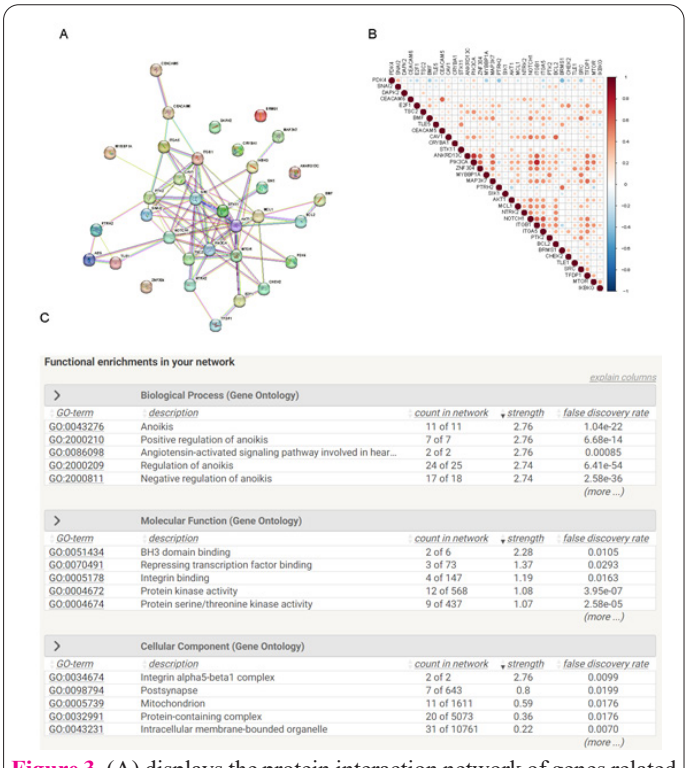

Functional enrichments in your network

Biological Process (Gene Ontology)

GO-term	description	count in network	strength	false discovery rate
GO:0043276	Anoikis	11 of 11	2.76	1.04e-22
GO:2000210	Positive regulation of anoikis	7 of 7	2.76	6.68e-14
GO:0086098	Angiotensin-activated signaling pathway involved in hear...	2 of 2	2.76	0.00085
GO:2000209	Regulation of anoikis	24 of 25	2.74	6.41e-54
GO:2000811	Negative regulation of anoikis	17 of 18	2.74	2.58e-36

(more ...)

Molecular Function (Gene Ontology)

GO-term	description	count in network	strength	false discovery rate
GO:0051434	BH3 domain binding	2 of 6	2.28	0.0105
GO:0070491	Repressing transcription factor binding	3 of 73	1.37	0.0293
GO:0005178	Integrin binding	4 of 147	1.19	0.0163
GO:0004672	Protein kinase activity	12 of 568	1.08	3.95e-07
GO:0004674	Protein serine/threonine kinase activity	9 of 437	1.07	2.58e-05

(more ...)

Cellular Component (Gene Ontology)

GO-term	description	count in network	strength	false discovery rate
GO:0034674	Integrin alpha5-beta1 complex	2 of 2	2.76	0.0099
GO:0098794	Postsynapse	7 of 643	0.8	0.0199
GO:0005739	Mitochondrion	11 of 1611	0.59	0.0176
GO:0032991	Protein-containing complex	20 of 5073	0.36	0.0176
GO:0043231	Intracellular membrane-bounded organelle	31 of 10761	0.22	0.0070

(more ...)

Figure 3. (A) displays the protein interaction network of genes related to anoikis, while (B) shows the Spearman correlation of these genes. (C) illustrates the Gene Ontology Biological Process enrichment of these genes.

resistance functional pathways, as shown in Figure 3C. Furthermore, we analyzed the correlation among all anoikis genes and found that there was a significant positive correlation between PIK3CA and ITGB1, as demonstrated in Figure 3B.

Molecular subtype identification based on anoikis genes in hepatocellular carcinoma

In this study, the TCGA-LIHC tumor samples were analyzed by consensus clustering based on the expression profiles of 34 anoikis-related genes. The CDF curve was close to flat when k=2 in the range of 0.1-0.9 (Figure 4A, B), indicating that the number of optimal clusters was 2. The samples were then divided into two subtypes, which had a relatively clear separation with clear boundaries, further verifying the stability of the clusters (Figure 4C). The differences in clinical characteristics were compared between the two subtypes, and it was found that there were significant differences in the prognostic survival curves of samples between subtypes (P<0.05) (Figure 4D). The prognosis of Cluster2 was good, and the prognosis of Cluster1 was poor. The study also analyzed the expression of anoikis-related genes in the two subtypes and found significant differences in their expressions. Additionally, differences in clinical characteristics such as age, clinical stage, and gender were compared between the two subtypes, and significant differences were found. Principal component analysis was carried out, and the study found that anoikis genes can divide the HCC samples into two clusters

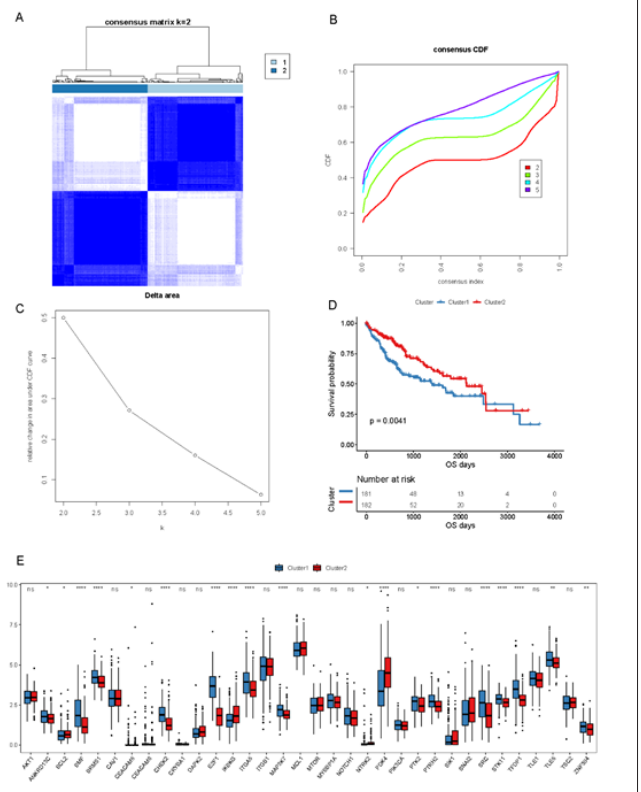

Figure 4. (A)displays patients were divided into two distinct gene clusters (C1and C2) by using consistent clustering (B)shows the cumulative distribution function when k takes different values(C)shows the relative change in area under the CDF curve between k and k-1(D) presents the KM curve between two subtypes, (E) shows the differential expression of anoikis genes between the two subtypes and clinical characteristics.

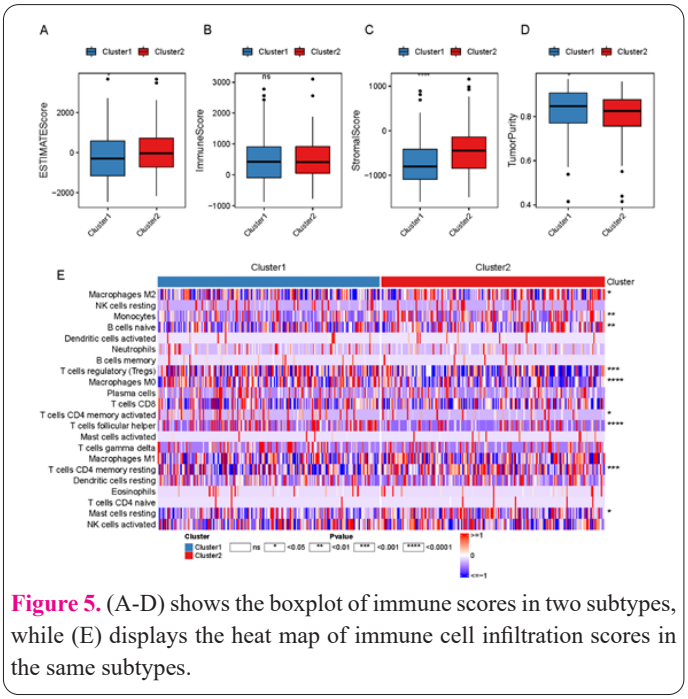

Figure 5. (A-D) shows the boxplot of immune scores in two subtypes, while (E) displays the heat map of immune cell infiltration scores in the same subtypes.

(Figure 4G), further verifying the accuracy of the study in dividing the samples into two subtypes.

Immune microenvironment infiltration among different subtypes of hepatocellular carcinoma

To investigate the correlation between anoikis subtypes and immune status, the 'ESTIMATE' package was used to analyze the differences in the immune score, stromal score, and tumor purity score in the two subtypes. The analysis revealed that there were differences in matrix score and tumor purity score between the two subtypes, with Cluster1 having a higher tumor purity score, as is illustrated in Figure 5. To further understand the differences in the tumor immune microenvironment of the two subtypes, the study employed the Cibersort package to determine the immune scores of the different molecular subtypes. The analysis showed that there was a significant difference in the infiltration scores of immune cells in the two subtypes, particularly the score of stromal cells. This finding highlights the close relationship between anoikis and extracellular matrix, and the differential expression was significant and similar to that of immune cells obtained from the Cibersort package among different subtypes.

Anoikis-related signature genes in hepatocellular carcinoma

To understand the biological functions of different subtypes, we calculated 742 differentially expressed genes between two anoikis subtypes of HCC using limma and performed enrichment analysis. The results of GO enrichment analysis revealed that the differentially expressed genes were mainly involved in biological processes such as chromosome segregation, mitotic nuclear division, and DNA replication. The KEGG enrichment analysis showed that these genes were mainly enriched in complement and coagulation cascades, cell cycle, drug metabolism-cytochrome P450, and other signaling pathways. For details, please refer to Figure 6 for the results.

Univariate Cox regression analysis was conducted on 742 differential genes between two subtypes. Out of these, 279 genes were screened and correlated with pro-

gnosis when the significance P value was less than 0.01. The top 6 genes were selected, and a KM map of top 6 was drawn. The high and low-risk groups were divided based on the median value of gene expression (refer to Figure 7). Using LASSO Cox, redundant genes were removed based on 279 prognostic-related genes, and 13 key prognostic genes were screened out (refer to Figure 8) (Table 1). A risk score for predicting sample survival was established by weighting the expression of these 13 genes and the LASSO regression coefficient. The model (where exp represents gene expression level, and coef represents

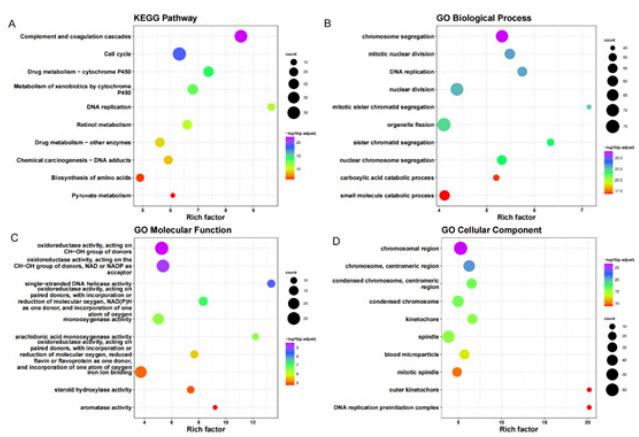

Figure 6. (A) KEGG enrichment; (B) GO BP enrichment; (C) GO MF enrichment; (D) GO CC enrichment.

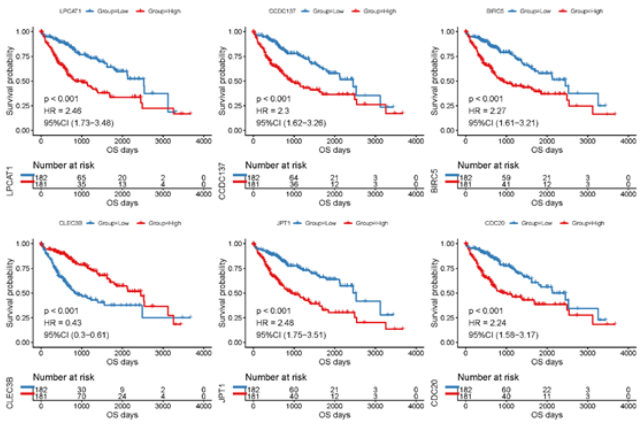

Figure 7. Top6 prognostic genes (high and low-risk groups are divided according to the median value).

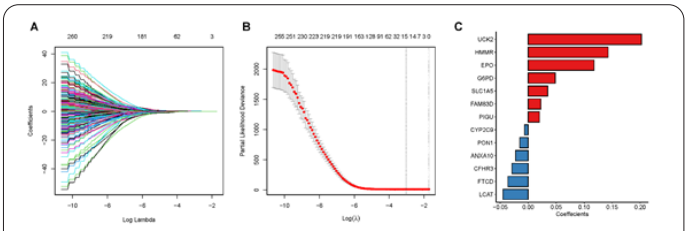

Figure 8. (A) shows the changing track of the independent variable of LASSO regression, where the abscissa represents the logarithm of the independent variable Lambda, and the ordinate represents the coefficient of the independent variable. (B) displays the confidence interval of each Lambda in the LASSO regression. Lastly, (C) illustrates the regression coefficient of the key prognostic gene LASSO.

LASSO regression coefficient) indicates that a regression coefficient greater than 0 indicates that the gene is a risk factor, and less than 0 indicates that the gene is a protective factor.

The study calculated the risk score of tumor samples using a risk score model and divided them into high and low risk score groups based on the median score. The prediction results were evaluated by ROC and showed that the prognosis of the high-risk group samples was worse in both the training set TCGA-LIHC and the independent data set GSE116174. The AUCs of the prediction results for 1 year, 3 years, and 5 years were also reported (Figures 9 and 10).

The study further conducted univariate and multivariate Cox regression analysis to explore the relationship between the prognostic value of the model and other clinical factors. The results showed that the constructed prognostic model was an independent prognostic factor ($P<0.05$).

In this study, the validation set GSE116174 was used to analyze the clinical characteristics (such as clinical stage and age) and risk score of a prognostic model through univariate and multivariate Cox regression analysis. The results indicate that the prognostic model is an independent prognostic factor ($P<0.05$, Figure 11). Additionally, the study examined the correlation between characteristic genes and clinical characteristics of patients in the training and validation sets, revealing differences in characteristic genes across different clinical characteristics.

Table 1. Key prognostic genes were identified in the study.

Signature gene	coef
UCK2	0.202490650859975
HMMR	0.14279845076107
CFHR3	-0.0290762840713765
PIGU	0.0199887821154947
CYP2C9	-0.00672281431509634
LCAT	-0.0450505301284314
SLC1A5	0.0348243861135984
G6PD	0.0485871491731648
ANXA10	-0.0227607156567921
PON1	-0.0150427022120064
FAM83D	0.0227473623863949
FTCD	-0.0362301041370092
EPO	0.117756570457452

Relationship between signature genes and the tumor microenvironment in hepatocellular carcinoma

Using TCGA-LIHC expression information, we employed ssGSEA to determine the enrichment score of tumor characteristic pathways and evaluate the characteristic pathways of group differences. We also compared the differences in 50 signature pathways between the high and low-risk score groups. Our results indicate significant differences in active oxygen pathway, late estrogen response pathway, myogenesis pathway, Wnt/β-catenin, and other pathways between high and low-risk score groups (Figure 12). Additionally, we calculated the immune score, stromal score, and tumor purity score using the ESTIMATE tool and displayed box plots (Figure 13E-H). Our findings revealed that the low-risk group had higher Stromal scores. Furthermore, we used the Cibersort method to calculate immune cell infiltration and found that the infiltration scores of immune cells such as macrophage M1, macrophage M2, and memory T cells in the low-risk group were significantly higher than those in the high-risk group ($P<0.05$, Figure 14I). The results of the Cibersort method were consistent with the ESTIMATE score, indicating a consistent immune trend between the two methods (Figure 13A-D).

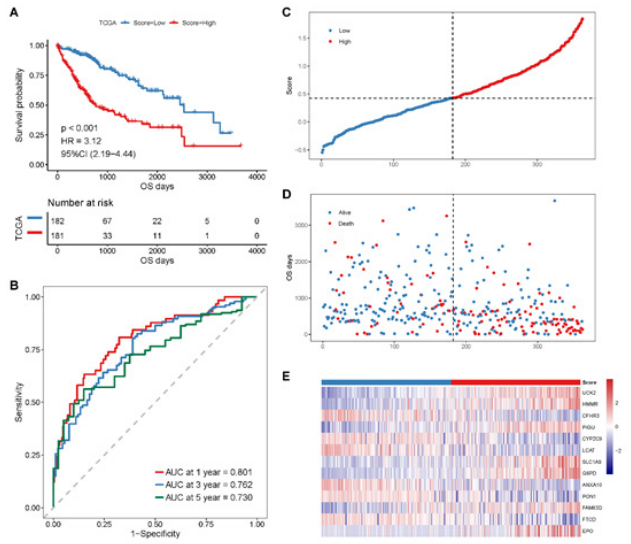

Figure 9. (A) shows a comparison of the prognosis between high and low-risk score groups. (B) displays the AUC curves of the risk score for 1-, 3-, and 5-year survival prediction. (C) and (D) depict the risk score sorted from small to large, with the abscissa indicating the sample. The vertical axis of (C) represents the risk score, while the vertical axis of (D) represents the survival time. Finally, (E) illustrates the z-score heat map of key prognostic gene expression. As the sample risk score increases, the expression level of each gene increases or decreases.

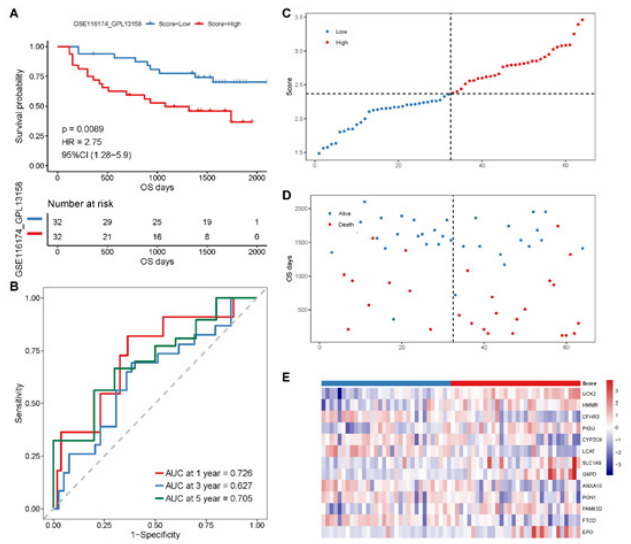

Figure 10. (A) shows a comparison of prognosis between high and low-risk score groups. (B) displays AUC curves of risk score for 1-, 3-, and 5-year survival prediction. In (C, D), the risk score is sorted from small to large, and the abscissa indicates the sample. The vertical axis of (C) represents the risk score, and the vertical axis of (D) represents the survival time. Finally, (E) shows the z-score heat map of key prognostic gene expression. As the risk score of the sample increases, the expression level of each gene increases/decreases.

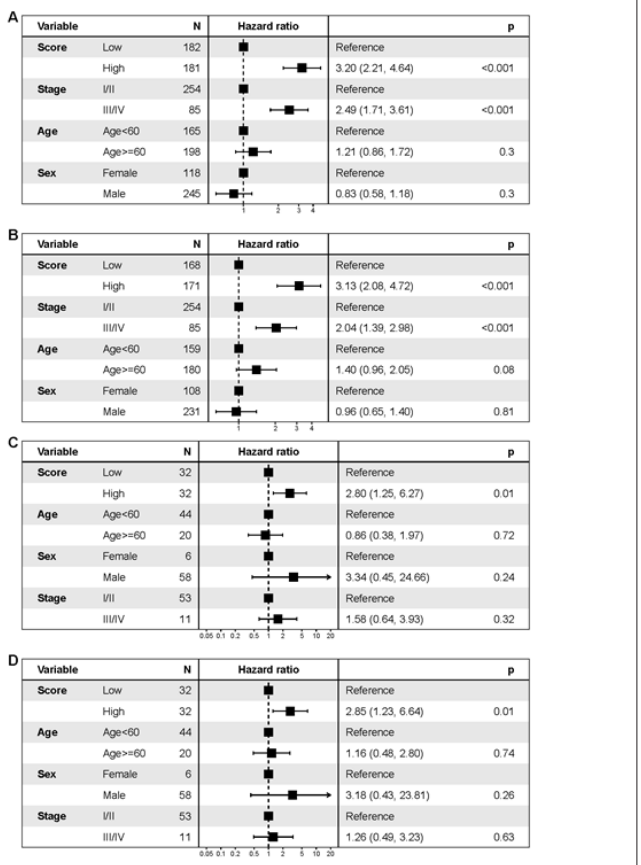

Figure 11. (A) shows the results of single factor Cox regression analysis, while (B) displays the multivariate Cox regression analysis. (C) depicts the single-factor Cox regression analysis, and (D) illustrates the multivariate Cox regression analysis.

Drug resistance among different risk score groups of hepatocellular carcinoma

The Genomics of Cancer Drug Sensitivity (GDSC) project identified many clinically active genes as targets of anticancer drugs, including EGFR. To evaluate the potential impact of risk score on drug response, the R package oncoPredict and the GDSC database drug information were used to predict the drug IC50 value of TCGA-LIHC data set samples. As shown in Figure 14, the correlation between IC50 value and risk score was calculated, and several drugs were compared, including Sorafenib, Cisplatin, Vorinostat, and Vinblastine. The study found significant differences in the IC50 values of these drugs between high and low-risk score groups. Specifically, the

Figure 12. Differences in characteristic pathways between high and low-risk score groups.

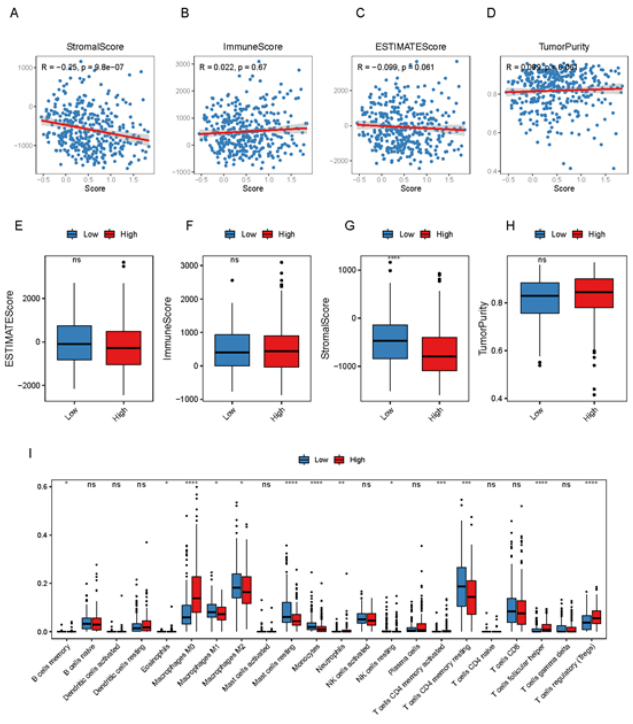

Figure 13. (A-H) shows the immune score, stromal score, and tumor purity score. The comparison of differences between the high and low-risk groups of immune-related cells is presented in section (I).

IC50 value of Vinblastine was significantly negatively correlated with the risk score, and its IC50 value was also significantly higher in the low-risk group. As is shown in Figure 14, these results suggest that patients in the high-risk group may be more sensitive to vincristine treatment, while anoikis resistance of tumor cells may lead to sorafenib resistance.

Discussion

Hepatocellular carcinoma is the most common type of primary liver cancer and the third leading cause of cancer-related death worldwide (7). The high metastasis rate and drug resistance of HCC lead to frequent tumor recurrence and poor prognosis. Therefore, we need to seek more effective treatment measures and detection methods to improve the survival time and prognosis of HCC patients. In recent years, systemic therapy has been the main treatment for advanced liver cancer; several drugs have been shown to have significant survival benefits as single agents, such as first-line drugs sorafenib and lenvatinib, second-line drugs regorafenib, Cabozantinib combined with ramucirumab, etc. Six recent systemic therapies based on phase 3 trials (atezolizumab plus bevacizumab, sorafenib, lenvatinib, regorafenib, cabozantinib plus ramucirumab) has been approved. In addition, there are currently ongoing clinical trials of various immune checkpoint inhibitors in combination with tyrosine kinase inhibitors or anti-VEGF therapies (1, 8). However, based on the existing treatment options, the objective response rate of patients is not ideal. The response rate of single immune checkpoint inhibitors (ICIs) treatment is only about 15-20% (9), while atezolizumab combined with The objective response rate with bevacizumab was 35.4% (10). Research has indicated that the acquisition of anoikis resistance in tumor cells may be linked to poor treatment outcomes for patients. A study using sorafenib to treat renal cell carcinoma found that the drug was less effective in Anoikis-resistant human renal carcinoma cells. Anoikis resistance allows HCC cells to evade immune surveillance and resist traditional chemotherapy drugs, keeping them alive in circulation and leading to metastatic lesions. Therefore, understanding the anti-apoptosis mechanism of HCC cells is crucial in preventing the invasion and metastasis of HCC cells.

Anoikis, a type of programmed cell death, is triggered when cells detach from the extracellular matrix (11). Anoikis resistance is a significant contributor to cancer progression and is linked to tumor metastasis and therapy resistance (12, 13). In the case of hepatocellular carcinoma, anoikis resistance is a key factor in tumor progression and recurrence, leading to poor prognosis and reduced survival rates (2). To better comprehend the interplay between tumor cells and the extracellular matrix, as well as the regulation mechanism of anoikis, we conducted an extensive study. In recent years, studies have found that certain factors or drugs inhibit the anoikis of liver cancer cells through some signaling pathways. These signaling pathways are not completely separated, but are interconnected and interact to promote liver cancer cell metastasis. One of the important signaling pathways is the PI3K/Akt/mTOR signaling pathway (14-16), which can regulate anoikis resistance in various ways. For example, Akt can directly or indirectly activate downstream effector molecules such as Bcl-2 family proteins, NF-κB and FOXO, thereby preventing mitochondrial outer membrane per-

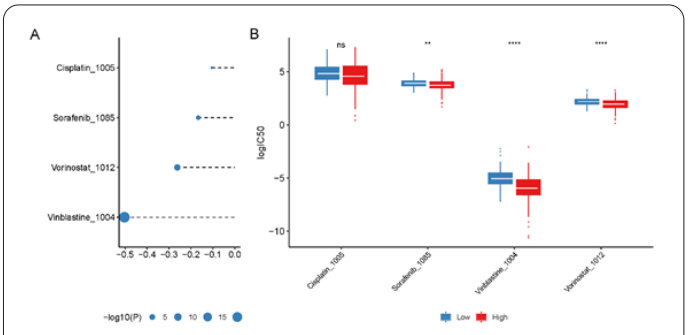

Figure 14. (A) displays the Spearman correlation between the risk score and drug IC50, while (B) shows the correlation of IC50 values with the high and low-risk groups.

meabilization and caspase activation (16, 17); mTOR can affect anoikis by regulating autophagy and metabolic balance (18); PI3K can affect cytoskeleton and nuclear stability by regulating Rho GTPase and polymeric nucleotide kinase (PAN) (19). The Wnt/β-catenin signaling pathway is a crucial pathway that regulates epithelial-mesenchymal transition, thereby promoting the proliferation, invasion, and migration of liver cancer cells by regulating multiple target genes (20, 21). One such example is the binding of β-catenin to TCF/LEF family transcription factors that activate the expression of c-Myc, cyclin D1, MMPs, and other genes in the nucleus (22-24). Additionally, Wnt can bind to Frizzled receptors and activate Rac/Rho GTPases and downstream molecules such as JNK (25, 26). In addition to the aforementioned signaling pathways, the MAPK/ERK signaling pathway is also involved in regulating anoikis resistance (27). This pathway has the ability to activate Bcl-2 family proteins, ring-finger protein 126, and other molecules, which in turn can protect liver cancer cells from undergoing anoikis.

Our study aimed to investigate the interaction between tumor cells and the extracellular matrix, as well as the regulation mechanism of anoikis. We analyzed 363 tumor tissue samples and 50 paracancerous tissue samples of TCGA-LIHC and discovered dysregulated expression of most anoikis genes. We then conducted consistency clustering analysis on the tumor samples of LIHC and divided the tissue samples into two subtypes. Our findings indicated that Cluster2 had a better prognosis. Further analysis of the immune infiltration of the two subtypes and the functional analysis of differentially expressed genes showed that Cluster2 had a better prognosis. The differential genes were mainly enriched in signaling pathways such as chromosome segregation, mitotic nuclear division, DNA replication, and cell cycle. Additionally, we observed a correlation between quality transformation and PI3K/Akt (16). To gain a further understanding of the biological functions of different subtypes, we calculated 742 differentially expressed genes between the two LIHC anoikis subtypes using limma and enriched them. We then performed univariate Cox regression analysis on the differential genes between subtypes and identified 279 genes that were significantly correlated with prognosis when the P value was less than 0.01. Next, we used LASSO Cox to remove redundant genes and identified 13 key prognostic genes. Among these genes, we found that high-risk genes are associated with the promotion of liver cancer development. Recent experimental findings have shed light on the mechanisms behind the development of HCC. UCK2 activates the EGFR-AKT pathway and promotes metastasis of HCC (28), while HMMR stimulates the development of nonalcoholic steatohepatitis and HCC through the CEBPα axis (29). PIGU activates the NF-κB pathway, leading to increased immune escape and drug resistance in HCC (30). SLC1A5 is a valuable predictor of HCC due to its role in ferroptosis (31). FAM83D is an important ERK-related gene that activates the MEK/ERK signaling pathway to promote liver cancer cell proliferation (32). Additionally, EPO promotes HCC cell proliferation through hypoxia-induced translocation of its specific receptors, leading to metastasis and drug resistance (33, 34). These findings support the reliability of the prognostic model indicators presented in this paper.

As mentioned before, we first developed the prognostic model and calculated the risk score to predict the survival time of each sample by weighing the expression of 13 genes with LASSO regression coefficients. The model's detection efficiency was verified through data from the training set TCGA-LIHC and the verification set GSE116174. We then used ssGSEA to calculate the enrichment score of tumor characteristic pathways based on the expression information of TCGA-LIHC. We evaluated differential pathways between groups and found that the differences between high and low-risk groups were primarily concentrated in the active oxygen pathway, late estrogen response pathway, myogenesis pathway, Wnt/β-catenin, and other pathways. These findings are consistent with existing research data. The studies conducted by Ma WL et al, Shimokawa M et al, and Li K et al have shown that hepatic androgen receptors, intracellular reactive oxygen species, and ZNF32 respectively play a role in regulating anoikis sensitivity in liver cancer cells. Ma WL et al found that hepatic androgen receptor can enhance anoikis and inhibit HCC cell migration by inhibiting p38 phosphorylation/activation and nuclear factor kappa B (NF-κB)/matrix metallopeptidase 9 (MMP9) pathway (35). Shimokawa M et al. found that increased intracellular reactive oxygen species (ROS) stimulated nuclear factor erythroid-derived 2 (Nrf2) and quinone oxidoreductase 1 (Nqo1), resulting in excessive oxidative stress and significantly increased anoikis sensitivity (36). This suggests that targeting Nqo1 activity may be a potential strategy for adjuvant therapy for liver cancer. Li K et al. found that ZNF32 promotes anoikis resistance by maintaining redox homeostasis and activating Src/FAK signaling (37). Wang W et al. discovered that overexpression of PRDX4 led to a decrease in β-TrCP-mediated β-catenin ubiquitination and an increase in β-catenin protein stability (20). This ultimately resulted in the activation of β-catenin signaling and resistance to anoikis. These findings suggest that targeting these pathways may be a potential avenue for adjuvant therapy in liver cancer. Finally, we selected several common clinical drugs for hepatocellular carcinoma, Sorafenib, Cisplatin, Vorinostat, and Vinblastine. We speculated that patients in the high-risk group may be Vincristine (Vinblastine) treatment is more sensitive. Additionally, tumor cells that exhibit anoikis resistance may also display resistance to sorafenib treatment (38).

Conclusion

Our study revealed that the majority of anoikis genes exhibited widespread dysregulation in the TCGA-LIHC cohort. Through consensus clustering, we were able to identify molecular subtypes and divided the samples into two subtypes that displayed significant prognostic differences. We then screened 13 key prognostic genes to develop a risk-scoring model, which demonstrated a high AUC value and strong predictive capabilities. Our drug efficacy prediction also showed promising results for the high-risk group.

Acknowledgment

This work was supported by the National Natural Science Foundation of China (grant no. 81871927).

Author Contributions

All authors contributed significantly to the reported work, whether that is in the conception, study design, execution,

acquisition of data, analysis and interpretation, or in all these areas; were involved in the drafting, review and revision of the article; gave final approval of the version to be published; have agreed on the journal to which the article has been submitted; and agree to be accountable for all aspects of the work.

Disclosure

The authors report no conflicts of interest in this work.

References

1. Gilles H, Garbutt T, Landrum J. Hepatocellular Carcinoma. Crit Care Nurs Clin 2022; 34(3): 289-301.
2. Yang C, Zhang H, Zhang L, et al. Evolving therapeutic landscape of advanced hepatocellular carcinoma. Nat Rev Gastro Hepat 2023; 20(4): 203-222.
3. Anstee QM, Reeves HL, Kotsiliti E, Govaere O, Heikenwalder M. From NASH to HCC: current concepts and future challenges. Nat Rev Gastro Hepat 2019; 16(7): 411-428.
4. Adeshakin FO, Adeshakin AO, Afolabi LO, Yan D, Zhang G, Wan X. Mechanisms for Modulating Anoikis Resistance in Cancer and the Relevance of Metabolic Reprogramming. Front Oncol 2021; 11: 626577.
5. Khan SU, Fatima K, Malik F. Understanding the cell survival mechanism of anoikis-resistant cancer cells during different steps of metastasis. Clin Exp Metastas 2022; 39(5): 715-726.
6. Fanfone D, Wu Z, Mammi J, et al. Confined migration promotes cancer metastasis through resistance to anoikis and increased invasiveness. Elife 2022; 11:
7. Lee TH, Mohta NS, Prewitt E, et al. NEJM Catalyst Innovations in Care Delivery - A New Journal Leading the Transformation of Health Care Delivery. New Engl J Med 2020; 382(1): 80-81.
8. Cheng AL, Hsu C, Chan SL, Choo SP, Kudo M. Challenges of combination therapy with immune checkpoint inhibitors for hepatocellular carcinoma. J Hepatol 2020; 72(2): 307-319.
9. Finn RS, Ryoo BY, Merle P, et al. Pembrolizumab As Second-Line Therapy in Patients With Advanced Hepatocellular Carcinoma in KEYNOTE-240: A Randomized, Double-Blind, Phase III Trial. J Clin Oncol 2020; 38(3): 193-202.
10. Finn RS, Qin S, Ikeda M, et al. Atezolizumab plus Bevacizumab in Unresectable Hepatocellular Carcinoma. New Engl J Med 2020; 382(20): 1894-1905.
11. Tan K, Goldstein D, Crowe P, Yang JL. Uncovering a key to the process of metastasis in human cancers: a review of critical regulators of anoikis. J Cancer Res Clin 2013; 139(11): 1795-1805.
12. Kakavandi E, Shahbahrami R, Goudarzi H, Eslami G, Faghihloo E. Anoikis resistance and oncoviruses. J Cell Biochem 2018; 119(3): 2484-2491.
13. Sattari FF, Jalilzadeh N, Mehdizadeh A, Sajjadian F, Velaei K. Understanding and targeting anoikis in metastasis for cancer therapies. Cell Biol Int 2023; 47(4): 683-698.
14. Sun B, Hu C, Yang Z, et al. Midkine promotes hepatocellular carcinoma metastasis by elevating anoikis resistance of circulating tumor cells. Oncotarget 2017; 8(20): 32523-32535.
15. LoRusso PM. Inhibition of the PI3K/AKT/mTOR Pathway in Solid Tumors. J Clin Oncol 2016; 34(31): 3803-3815.
16. de Sousa MA, de Araujo LS, Pernambuco FP, Nader HB, Lopes CC. Acquisition of anoikis resistance promotes alterations in the Ras/ERK and PI3K/Akt signaling pathways and matrix remodeling in endothelial cells. Apoptosis 2017; 22(9): 1116-1137.
17. Lu M, Hartmann D, Braren R, et al. Oncogenic Akt-FOXO3 loop favors tumor-promoting modes and enhances oxidative damage-associated hepatocellular carcinogenesis. Bmc Cancer 2019; 19(1): 887.
18. Patra T, Bose SK, Kwon YC, Meyer K, Ray R. Inhibition of p70 isoforms of S6K1 induces anoikis to prevent transformed human hepatocyte growth. Life Sci 2021; 265: 118764.
19. Song W, Chen J, Li S, et al. Rho GTPase Activating Protein 9 (ARHGAP9) in Human Cancers. Recent Pat Anti-Canc 2022; 17(1): 55-65.
20. Wang W, Shen XB, Huang DB, Jia W, Liu WB, He YF. Peroxiredoxin 4 suppresses anoikis and augments growth and metastasis of hepatocellular carcinoma cells through the beta-catenin/ID2 pathway. Cell Oncol 2019; 42(6): 769-781.
21. Parsons MJ, Tammela T, Dow LE. WNT as a Driver and Dependency in Cancer. Cancer Discov 2021; 11(10): 2413-2429.
22. Gao H, Yin FF, Guan DX, et al. Liver cancer: WISP3 suppresses hepatocellular carcinoma progression by negative regulation of beta-catenin/TCF/LEF signalling. Cell Proliferat 2019; 52(3): e12583.
23. Yang TW, Gao YH, Ma SY, Wu Q, Li ZF. Low-grade slightly elevated and polypoid colorectal adenomas display differential beta-catenin-TCF/LEF activity, c-Myc, and cyclin D1 expression. World J Gastroentero 2017; 23(17): 3066-3076.
24. Katoh M, Katoh M. WNT signaling and cancer stemness. Essays Biochem 2022; 66(4): 319-331.
25. Ma Y, Wang S, Wu Y, et al. Hepatic stellate cell mediates transcription of TNFSF14 in hepatocellular carcinoma cells via H(2)S/CSE-JNK/JunB signaling pathway. Cell Death Dis 2022; 13(3): 238.
26. Bugter JM, Fenderico N, Maurice MM. Mutations and mechanisms of WNT pathway tumour suppressors in cancer. Nat Rev Cancer 2021; 21(1): 5-21.
27. Yoshino S, Hara T, Nakaoka HJ, et al. The ERK signaling target RNF126 regulates anoikis resistance in cancer cells by changing the mitochondrial metabolic flux. Cell Discov 2016; 2(16019.
28. Cai J, Sun X, Guo H, et al. Non-metabolic role of UCK2 links EGFR-AKT pathway activation to metastasis enhancement in hepatocellular carcinoma. Oncogenesis 2020; 9(12): 103.
29. Zhang D, Liu J, Xie T, et al. Oleate acid-stimulated HMMR expression by CEBPalpha is associated with nonalcoholic steatohepatitis and hepatocellular carcinoma. Int J Biol Sci 2020; 16(15): 2812-2827.
30. Wei X, Yang W, Zhang F, Cheng F, Rao J, Lu L. PIGU promotes hepatocellular carcinoma progression through activating NF-kappaB pathway and increasing immune escape. Life Sci 2020; 260: 118476.
31. Su H, Liu Y, Huang J. Ferroptosis-Related Gene SLC1A5 Is a Novel Prognostic Biomarker and Correlates with Immune Microenvironment in HBV-Related HCC. J Clin Med 2023; 12(5):
32. Wang D, Han S, Peng R, et al. FAM83D activates the MEK/ERK signaling pathway and promotes cell proliferation in hepatocellular carcinoma. Biochem Bioph Res Co 2015; 458(2): 313-320.
33. Li Z, Kwon SM, Li D, et al. Human constitutive androstane receptor represses liver cancer development and hepatoma cell proliferation by inhibiting erythropoietin signaling. J Biol Chem 2022; 298(5): 101885.
34. Miao S, Wang SM, Cheng X, et al. Erythropoietin promoted the proliferation of hepatocellular carcinoma through hypoxia induced translocation of its specific receptor. Cancer Cell Int 2017; 17: 119.
35. Ma WL, Hsu CL, Yeh CC, et al. Hepatic androgen receptor suppresses hepatocellular carcinoma metastasis through modulation of cell migration and anoikis. Hepatology 2012; 56(1): 176-185.
36. Shimokawa M, Yoshizumi T, Itoh S, et al. Modulation of Nqo1 activity intercepts anoikis resistance and reduces metastatic potential of hepatocellular carcinoma. Cancer Sci 2020; 111(4):

1228-1240.

37. Li K, Zhao G, Ao J, et al. ZNF32 induces anoikis resistance through maintaining redox homeostasis and activating Src/FAK signaling in hepatocellular carcinoma. Cancer Lett 2019; 442: 271-278.

38. Zhang P, Xing Z, Li X, et al. Tyrosine receptor kinase B silencing inhibits anoikis-resistance and improves anticancer efficiency of sorafenib in human renal cancer cells. Int J Oncol 2016; 48(4): 1417-1425.